Statistical fragmentation of small neutral carbon clusters

S. Díaz-Tendero,[1] P.-A. Hervieux,[2] M. Alcamí,[1] and F. Martín[1]

[1]*Departamento de Química, C-9, Universidad Autónoma de Madrid, 28049 Madrid, Spain*
[2]*Institut de Physique et Chimie des Matériaux de Strasbourg, GONLO, 23 rue du Loess, 67034 Strasbourg, France*

We present a statistical fragmentation study of the C_5, C_7, and C_9 carbon clusters using the Metropolis Monte Carlo and Weisskopf methods. We show that inclusion of several isomeric forms as well as rotational effects is essential to reproduce the experimental observations. We have found that, for cluster excitation energies around 10 eV, several fragmentation channels are efficiently populated, but the dominant one always corresponds to C_{n-3}/C_3. For high enough excitation energies, we observe first-order phase transitions corresponding to a complete breakup of the cluster.

I. INTRODUCTION

Fragmentation is the dominant deexcitation channel of highly excited carbon clusters [1,2]. Thus the analysis of the different dissociation channels can provide information on the stability of these clusters as well as on the dynamics of the excitation process [3–5]. In the particular case of small carbon clusters, fragmentation has been studied using different experimental approaches. The unimolecular decay of C_n^+ formed in a direct vaporization source has been extensively studied by Radi *et al.* [6–8]. Photofragmentation experiments of jet-cooled cationic clusters have been performed by Geusic *et al.* [9–11] and by Bouyer *et al.* [12]. Fragmentation of C_n^+ clusters has been also investigated in collision induced dissociation (CID) experiments [13,14] and through mass-analyzed ion kinetic energy spectra (MIKES) [15–17]. In addition, fragmentation of negatively charged C_n^- clusters have been studied in CID [18] and in surface-induced dissociation (SID) experiments [19]. In these experiments, the loss of neutral C_3 has been found to be the dominant dissociation process for both positive and negative cluster ions.

Although charged carbon clusters have been extensively studied, the experimental information for fragmentation of neutral carbon clusters is scarce. Choi *et al.* [20] have studied photodissociation of linear neutral carbon clusters. Chabot *et al.* [21] have performed experiments in which excited neutral clusters are produced by electron capture in fast $C_n^+ + He$ collisions. In the latter experiments, the decay of the excited cluster leads to a large number of fragmentation channels. The corresponding branching ratios were quantitatively determined for sizes up to $n=9$.

When clusters are excited by laser pulses, fast electrons or fast heavy particles, the excitation process is much faster than the internal motion of the cluster nuclei. Thus the excitation energy is redistributed among the cluster vibrational degrees of freedom well after the electronic excitation has taken place. Consequently, one can treat cluster fragmentation as a postcollisional process. Most previous works have described the time evolution of the excited clusters by means of molecular dynamics (MD) methods [22]. In these methods, a critical aspect is the description of the atom-atom interactions that govern the nuclear dynamics. This can be

done by means of (i) simple analytical two-body interaction potentials or (ii) *ab initio* interaction potentials obtained on the "fly" [23]. The second approach is very much limited by cluster size. However, we know from previous studies that the dynamical evolution of a complicated many-body system is mainly guided by the accessible phase space [24]. Thus a statistical treatment may explain the outcome of such fragmentation reactions. This is particularly important for large systems, since statistical methods are computationally much cheaper than MD methods.

In this work we have adapted two statistical methods, initially proposed to study fragmentation of hot atomic metal clusters [25,26], to investigate fragmentation of highly excited small neutral carbon clusters. The first method is the microcanonical Metropolis Monte Carlo (MMMC) method, which consists in partitioning the mass, charge, total energy, total linear, and angular momenta of the system (conserved in the microcanonical approach) among all possible final channels with probabilities governed by considerations of maximum entropy. The second method considers a sequential evaporation chain with rate constants calculated within the statistical Weisskopf theory. The basic ingredients of both methods are binding energies, geometries, vibrational frequencies, and rotational constants of any possible fragment. This information must be extracted from *ab initio* quantum chemistry calculations. Although several authors have studied the properties of small carbon clusters [27–35], the quantitative information available in the literature has been obtained at different levels of theory (see [36] and references therein). To avoid possible inconsistencies due to the use of different *ab initio* methods and to evaluate the missing parameters, we have consistently calculated all microscopic properties using the same level of theory for all possible fragments.

In a recent Letter [5] we have used the results of MMMC calculations to extract the energy distribution of C_n neutral carbon clusters produced by charge transfer reactions in C_n^+ collision experiments. This combination of experimental measurements with theory allows one to extract information on the collision dynamics that would be extremely difficult to obtain from theory or experiment alone. In this work we will focus our attention on the fragmentation process itself, irrespective of the excitation mechanism that leads to frag-

mentation, as well as on the details of the present implementation of the MMMC method. In particular, we will analyze under which circumstances a statistical treatment based on the ergodic assumption is meaningful to analyze fragmentation observed in a finite time interval (the time of flight of the experiments). Furthermore, we will discuss to what extent the different microscopic properties of the C_n clusters affect the different fragmentation pathways as well as the possibility to observe phase transitions when the C_n excitation energy is varied. The present MMMC calculations slightly improve on those reported in [5] since statistical weights due to electronic orbital degeneracies are taken into account.

The paper is organized as follows. In the next two sections we explain in detail our implementation of the MMMC and Weisskopf methods to investigate fragmentation of small carbon clusters. In Sec. IV we summarize the theory and results of the quantum chemistry calculations that provide the necessary microscopic information to apply the above statistical methods. In Sec. V we present and discuss our results for the fragmentation of C_5, C_7, and C_9 clusters. We analyze in detail the influence of the different microscopic properties as well as the validity conditions of such theoretical treatments. A brief summary of the comparison between the calculated branching ratios and those recently measured by Martinet *et al.* [5] will be given in Sec. VI. We end the paper with some conclusions in Sec. VII. Atomic units are used throughout unless otherwise specified.

II. THE MICROCANONICAL METROPOLIS MONTE CARLO METHOD

The MMMC method was originally developed for the study of thermodynamics in nuclear physics [37] and has been successfully applied to study fragmentation of hot metal clusters [25]. The basic idea of the method is to move in phase space until a region of maximum entropy is reached. Then a physical observable is measured by performing a statistical average in this region. This method considers the system in internal thermodynamic equilibrium and, therefore, it cannot provide information on the time evolution of the system. In our implementation of the MMMC method we allow for all possible decay channels under the constraint of conservation of mass, charge, energy, linear momentum, and angular momentum.

A. The microcanonical ensemble

The physical quantity we are interested in is the statistical average of an observable F over the microcanonical ensemble

$$\langle F \rangle = \frac{\displaystyle\int_{\Omega'} F(\mathbf{x}')w(\mathbf{x}')d\mathbf{x}'}{\displaystyle\int_{\Omega'} w(\mathbf{x}')d\mathbf{x}'}, \qquad (1)$$

where $\mathbf{x}'$ represents a state (also called a configuration or a point) in phase space Ω', $w(\mathbf{x}')/\int_{\Omega'} w(\mathbf{x}')d\mathbf{x}'$ is the prob-

ability distribution of the microcanonical ensemble, and $\mathcal{Z} = \int_{\Omega'} w(\mathbf{x}')d\mathbf{x}'$ is the partition function. In our model, a phase space point $\mathbf{x}'$ is defined as

$$\mathbf{x}' = \{N_f; \{N_j, Z_j, S_{ej}, O_{ej}, G_j\}_{j=1}^{N_f}; \{\mathbf{r}_j\}_{j=1}^{N_f}; \{\mathbf{p}_j\}_{j=1}^{N_f};$$
$$\{\phi_j\}_{j=1}^{N_f}; \{\mathbf{l}_j\}_{j=1}^{N_f}; \{E_{vj}^*\}_{j=1}^{N_f}\}, \qquad (2)$$

where N_f is the number of fragments, $\{N_j, Z_j, S_{ej}, O_{ej}, G_j\}_{j=1}^{N_f}$ is the mass, the charge, the electronic spin, the electronic orbital degeneracy and the geometry (atomic, linear or cyclic) of each fragment with the constraint (mass and charge conservation)

$$\sum_{j=1}^{N_f} N_j = N_T,$$

$$\sum_{j=1}^{N_f} Z_j = Z_T. \qquad (3)$$

The initial cluster has N_T carbon atoms and a net charge Z_T (in this section the notation $C_{N_T}^{Z_T}$ will be used). $\mathbf{r}_j$ is the position (chosen such that fragments do not overlap each other; see Sec. II B 2), $\mathbf{p}_j$ is the linear momentum, ϕ_j are the rotational angles that determine the space orientation (2 for a linear molecule and 3 for nonlinear species), $\mathbf{l}_j$ is the angular momentum, and E_{vj}^* is the internal vibrational excitation energy of the fragment labeled j. In the present study, all fragments are neutral ($Z_j=0$ for all j) and are assumed to be in their electronic ground state.

In the microcanonical ensemble the total energy of the system is conserved and is fixed to be E_0 with

$$E_0 = E_C + E_b + E_v^* + K_t + K_r,$$

$$E_C = \sum_{j<i} \frac{Z_i Z_j}{|\mathbf{r}_i - \mathbf{r}_j|},$$

$$E_b = \sum_{j=1}^{N_f} E_{bj},$$

$$E_v^* = \sum_{j=1}^{N_f} E_{vj}^*,$$

$$K_t = \sum_{j=1}^{N_f} \frac{\mathbf{p}_j^2}{2m_j},$$

$$K_r = \sum_{j=1}^{N_f} \left(\sum_{\nu=1}^{f_{rj}} \frac{\mathbf{l}_{\nu j}^2}{2I_{\nu j}} \right), \qquad (4)$$

where E_C is the total Coulomb interaction energy between the fragments, i.e., zero in the present application, E_{bj} is the total electronic energy, $\mathbf{p}_j^2/2m_j$ the translational kinetic energy (K_t), $\sum_{\nu=1}^{f_{rj}} \mathbf{l}_{\nu j}^2/2I_{\nu j}$ the rotational kinetic energy (K_r), f_{rj}

the number of rotational degrees of freedom,[11] m_j the mass, and I_{vj} the principal moment of inertia ν of fragment j.

B. The microcanonical weights

In the microcanonical ensemble, the total energy, total linear momentum and total angular momentum are constant. Furthermore, due to the finite size of the system, the total number of atoms and the charge are fixed by the initial cluster size (N_T) and net charge (Z_T). Consequently, the microcanonical weight is given by [25]

$$
\begin{aligned}
w(\mathbf{x}')d\mathbf{x}' &= \delta(E - E_0)\delta(\mathbf{P} - \mathbf{P}_0)\delta(\mathbf{L} - \mathbf{L}_0) \\
&\quad \times \delta(N - N_T)\delta(Z - Z_T)d\mathbf{x}',
\end{aligned}
\tag{5}
$$

where

$$
\mathbf{P} = \sum_j^{N_f} \mathbf{p}_j
\tag{6}
$$

and

$$
\mathbf{L} = \sum_j^{N_f} \mathbf{l}_j + \sum_j^{N_f} (\mathbf{r}_j - \mathbf{R}_{c.m.}) \times (\mathbf{P}_j - \mathbf{P}_0).
\tag{7}
$$

$\mathbf{L}_0$ and $\mathbf{P}_0$ are, respectively, the cluster initial total angular momentum and linear momentum. $\mathbf{R}_{c.m.}$ denotes the position of the center of mass of the system. According to the definition (2), the volume element of the phase space is expressed as

$$
\begin{aligned}
d\mathbf{x}' &= \left(\prod_{j=1}^{N_f} \frac{d^3\mathbf{r}_j d^3\mathbf{p}_j}{(2\pi\hbar)^3}\right)\left(\prod_{j=1}^{N_f} \frac{d^{f_{rj}}\phi_j d^{f_{rj}}\mathbf{l}_j}{(2\pi\hbar)^{f_{rj}}\sigma_{rj}}\right) \\
&\quad \times \left(\prod_{j=1}^{N_f} \rho_{vj}(E_{vj}^*)dE_{vj}^*\right),
\end{aligned}
\tag{8}
$$

where σ_{rj} is the symmetry number of the fragment j (see Sec. II B 1) and $\rho_{vj}(E_{vj}^*)$ is the density of vibrational states of the fragment j at energy E_{vj}^*. It is also worth noting that $\mathbf{p}_j$ is the conjugated variable of $\mathbf{r}_j$ and $\mathbf{l}_j$ the conjugated variable of ϕ_j. The statistical average defined in Eq. (1) can now be written more explicitly as

$$
\begin{aligned}
\langle F \rangle &= \frac{1}{\mathcal{Z}} \sum_{N_f=1}^{N_T} w_{NZ}(N_f)\left[\sum_i^{N_{GS}} w_e(G_i, S_{ei}, O_{ei})\right. \\
&\quad \times \int F(\mathbf{x}')\delta(E - E_0)\delta(\mathbf{P} - \mathbf{P}_0)\delta(\mathbf{L} - \mathbf{L}_0) \\
&\quad \times \eta(\mathbf{r}_1, \mathbf{r}_2 \ldots \mathbf{r}_{N_f})\prod_{j_i=1}^{N_f} \frac{d^3\mathbf{r}_{j_i} d^3\mathbf{p}_{j_i}}{(2\pi\hbar)^3} \\
&\quad \left. \times \prod_{j_i=1}^{N_f} \frac{d^{f_{rj_i}}\phi_{j_i} d^{f_{rj_i}}\mathbf{l}_{j_i}}{(2\pi\hbar)^{f_{rj_i}}\sigma_{rj_i}} \prod_{j_i=1}^{N_f} \rho_{vj}(E_{vj_i}^*)dE_{vj_i}^*\right],
\end{aligned}
\tag{9}
$$

where N_{GS} is the number of channels for a given number of

fragments N_f (including all possible geometries and spin multiplicities), w_{NZ} is the number of ordered partitions of a cluster of N_T atoms and charge Z_T into N_f fragments [it results from integration of the $\delta(N-N_T)$ and $\delta(Z-Z_T)$ terms in Eq. (5)] [38]

$$
w_{NZ}(N_f) = \frac{1}{N_f!}\binom{N_T - 1}{N_f - 1}\binom{Z_T + N_f - 1}{N_f - 1},
$$

w_e is the degeneracy of the electronic ground state

$$
w_e(G_i, S_{ei}, O_{ei}) = \prod_{j=1}^{N_f} (2S_{ej} + 1)O_{ej},
\tag{10}
$$

and $\eta(\mathbf{r}_1 \ldots \mathbf{r}_{N_f})$ is a factor that takes into account the overlap in space of the fragments (see Sec. II B 2). The index i in Eq. (9) is a short notation for i_{N_f} where N_f runs from 1 to N_T.

According to Eqs. (1) and (9), the weight w can be split into the following factors:

$$
w = \sum_{N_f=1}^{N_T} w_{NZ}(N_f)\sum_i w_{e_i}w_{\phi_i}w_{r_i}w_{q_i}w_{pl_i}.
\tag{11}
$$

1. The weight w_ϕ

This weight factor due to the angular part of the eigenrotation of the fragments is given by

$$
w_\phi = \prod_{j=1}^{N_f} \int \frac{d^{f_{rj}}\phi_j}{(2\pi\hbar)^{f_{rj}}\sigma_{rj}}.
\tag{12}
$$

If we consider fragments with linear and cyclic geometry (single atom fragments are not included because they do not have rotational structure) we have

$$
w_\phi = \prod_{j=1}^{N_l} \int \frac{d^2\phi_j}{(2\pi\hbar)^2\sigma_{rj}} \prod_{i=1}^{N_c} \int \frac{d^3\phi_i}{(2\pi\hbar)^3\sigma_{ri}},
\tag{13}
$$

where N_l is the number of linear fragments and N_c is the number of fragments with cyclic geometry. σ_{ri} is the symmetry number of the fragment i. This quantity is introduced in statistical mechanics in order to reduce the rotational entropy of symmetric molecules and depends on the symmetry group [39] (see also Table I). The integration of Eq. (13) leads to

$$
w_\phi = \left(\frac{1}{\sigma_r^l}\right)^{N_l}\left\{\prod_{i=1}^{N_c}\left(\frac{1}{\sigma_{ri}}\right)\right\}\left(\frac{1}{\pi}\right)^{N_c+N_l}\left(\frac{1}{\hbar}\right)^{3N_c+2N_l}.
\tag{14}
$$

The symmetry number for linear fragments of $D_{\infty h}$ symmetry is $\sigma_r^l = 2$.

2. The weight w_r

In using the MMMC model we must simulate the accessible phase-space corresponding to fragments whose mutual interaction (Van der Waals forces and exchange of atoms) is negligible. Thus we simulate the fragmenting configurations within a spherical volume of radius $R_{sys} = r_f N_T$, where $r_f = 2$ Å. This volume is large enough to contain all isomeric

---

[1]For a single carbon atom, $f_{rj} = 0$, since this fragment is considered as a particle with no internal rotational structure.

TABLE I. Mass table: j is the fragment's label; N is the cluster size; G indicates the geometry (A, atomic specie; L, linear geometry; C, cyclic geometry) and the symmetry; $\mathcal{S}_e \equiv 2S_e+1$ is the electronic spin multiplicity; O_e is the electronic orbital multiplicity; σ_r is the symmetry number appearing in the weight factor due to the eigenrotation of the fragments (see [39]); $E+ZPE$ is the electronic energy obtained at the CCSD(T)/6−311+G(3df) level over the B3LYP geometry and the zero point energy correction obtained at the B3LYP/6−311+G(3df); $\bar{\nu}$ is the geometrical average of the vibrational frequencies given by $(\Pi_{i=1}^{f_{vj}} \nu_{ij})^{1/f_{vj}}$ where f_{vj} is the number of vibrational degrees of freedom ($f_{vj}=3N_j-5$ for linear species and $f_{vj}=3N_j-6$ for cyclic species); I_1, I_2, and I_3 are the principal moments of inertia; R is the radius of the fragment defined as half the largest distance between two C cluster atoms; D is the lowest dissociation energy corresponding to the fission channel with labels (l,k). Finally, $\ln(\rho)$ is related to the w_q factor with $\rho_j = D^{f_{vj}-1}/(\Gamma(f_{vj})\bar{\nu}_j^{f_{vj}})$.

j	N	G	$\mathcal{S}_e$	O_e	σ_r	$E+ZPE$ (a.u.)	$\bar{\nu}$(eV)	I_1/m_0 (Å²)	I_2/m_0 (Å²)	I_3/m_0 (Å²)	R(Å)	D(eV) (l,k)	$\ln(\rho)$
1	1	A	1	5	0	−37.72589	0.000000	0.0000	0.0000	0.0000	0.76720	0.00000	0.00000
2	1	A	3	3	0	−37.77917	0.000000	0.0000	0.0000	0.0000	0.76720	0.00000	0.00000
3	2	$L(D_{\infty h})$	1	1	2	−75.77837	0.232200	2.7764	2.7764	0.0000	0.62350	5.98737 (2,2)	3.24981
4	2	$L(D_{\infty h})$	3	2	2	−75.75791	0.209800	3.0233	3.0233	0.0000	0.65050	5.43062 (2,2)	3.25365
5	3	$L(D_{\infty h})$	1	1	2	−113.82422	0.049062	11.8262	11.8262	0.0000	1.28700	7.25679 (2,3)	19.29329
6	3	$L(D_{\infty h})$	3	2	2	−113.74810	0.047823	11.8891	11.8891	0.0000	1.29000	5.18544 (2,3)	18.05127
7	3	$C(C_{2v})$	1	1	2	−113.78543	0.176400	2.8124	4.1746	6.9870	0.88300	6.20125 (2,3)	10.67926
8	3	$C(D_{3h})$	3	1	6	−113.79267	0.161110	3.3192	3.3192	6.6384	0.78700	6.39826 (2,3)	11.04509
9	4	$L(D_{\infty h})$	1	1	2	−151.76200	0.067399	30.1371	30.1371	0.0000	1.95050	4.31603 (2,5)	24.32874
10	4	$L(D_{\infty h})$	3	1	2	−151.73920	0.068026	30.0438	30.0438	0.0000	1.94950	3.69561 (2,5)	23.17758
11	4	$C(D_{2h})$	1	1	4	−151.78067	0.099871	3.9768	10.8631	14.8399	1.23300	4.82407 (2,5)	20.08692
12	4	$C(D_{2h})$	3	1	4	−151.74738	0.089866	4.4024	10.1261	14.5285	1.19100	3.91820 (2,5)	19.47235
13	5	$L(D_{\infty h})$	1	1	2	−189.81595	0.066190	58.4789	58.4789	0.0000	2.56000	5.80587 (3,5)	34.13635
14	5	$L(D_{\infty h})$	3	2	2	−189.73064	0.078498	58.3638	58.3638	0.0000	2.55000	3.48445 (3,5)	27.32531
15	5	$C(C_s)$	1	1	1	−189.64652	0.137100	8.3280	14.8329	22.9043	1.33200	1.19541 (3,5)	10.96461
16	5	$C(C_2)$	3	1	1	−189.70491	0.093690	6.9822	17.7999	23.9031	1.45100	2.78429 (3,5)	22.00066
17	6	$L(D_{\infty h})$	1	1	2	−227.77243	0.063565	103.1003	103.1003	0.0000	3.21550	3.37397 (5,5)	34.13085
18	6	$L(D_{\infty h})$	3	1	2	−227.77657	0.064024	102.9515	102.9515	0.0000	3.21350	3.48662 (5,5)	34.46429
19	6	$C(D_{3h})$	1	1	6	−227.79560	0.111200	17.9057	17.9160	35.8216	1.46380	4.00446 (5,5)	27.90159
20	6	$C(C_{2v})$	3	1	2	−227.70536	0.098552	16.2726	21.4667	37.7393	1.56460	1.54888 (5,5)	17.95206
21	7	$L(D_{\infty h})$	1	1	2	−265.80739	0.061928	162.9505	162.9501	0.0000	3.83300	5.51035 (5,11)	46.62335
22	7	$L(D_{\infty h})$	3	2	2	−265.73061	0.058380	165.1399	165.1399	0.0000	3.85650	3.42104 (5,11)	39.94042
23	7	$C(C_{2v})$	1	1	2	−265.78847	0.090119	22.6989	33.2893	55.9883	1.67900	4.99551 (5,11)	37.67528
24	7	$C(C_{2v})$	3	1	2	−265.76765	0.077859	24.4609	33.4754	57.9363	1.71200	4.42896 (5,11)	38.06315
25	8	$L(D_{\infty h})$	1	1	2	−303.77373	0.059952	245.5097	245.5097	0.0000	4.48450	4.56671 (5,13)	48.82201
26	8	$L(D_{\infty h})$	3	1	2	−303.77354	0.060272	245.2952	245.2952	0.0000	4.48250	4.55992 (5,13)	48.69259
27	8	$C(C_{4h})$	1	1	8	−303.78713	0.084327	40.3222	40.3222	80.6444	1.83700	5.00256 (5,13)	42.82220
28	8	$C(D_{4h})$	3	1	8	−303.76604	0.077042	39.9843	40.0037	79.9880	1.83000	4.34923 (5,13)	41.92940
29	9	$L(D_{\infty h})$	1	1	2	−341.80020	0.059335	348.2156	348.2156	0.0000	5.10648	6.00668 (5,19)	59.24780
30	9	$L(D_{\infty h})$	3	1	2	−341.76339	0.054610	351.4200	351.4200	0.0000	5.13403	1.91333 (5,19)	35.90483
31	9	$C(C_s)$	3	1	1	−341.79248	0.069421	56.0323	57.1993	112.4990	2.03993	2.59147 (5,19)	36.67573
32	9	$C(C_s)$	3	3	1	−341.78741	0.073154	55.2419	58.2259	113.4680	2.04124	2.28561 (5,19)	32.93837

forms of the C_{N_T} cluster and all its fragments, since the diameter of the sphere is roughly four times larger than the length of the C_{N_T} cluster in its linear configuration. The quantity R_{sys} is called the freeze-out radius. We want to mention in advance that the results of our calculations are practically independent of R_{sys} provided it is large enough to contain all fragments (e.g., we have found that the results are practically the same for $r_f = 1$ Å).

The weight factor w_r is related to the spatial occupation of the fragments. It is defined as the accessible volume for each fragment and can be expressed as

$$w_r = \prod_{j=1}^{N_f} \int_{V_j} \eta(\mathbf{r}_1, \mathbf{r}_2, \dots, \mathbf{r}_{N_f}) \frac{1}{(2\pi\hbar)^3} d^3\mathbf{r}_j, \qquad (15)$$

where

$$\eta(\mathbf{r}_1, \mathbf{r}_2, \dots, \mathbf{r}_{N_f}) = \begin{cases} 1, & r_{lk} = |\mathbf{r}_l - \mathbf{r}_k| \geq R_l + R_k, l \neq k, \\ 0, & \text{otherwise.} \end{cases}$$
$$(16)$$

The factor η is introduced in order to avoid the overlapping between two fragments. The fragment's radius, R_l, is defined as half the largest distance between two cluster atoms (see Table I). V_j is the volume that the jth fragment can occupy in the empty freeze-out volume $V_j = \frac{4}{3}\pi(R_{sys} - R_j)^3$.

This weight plays a very important role in the fragmentation of multiply charged clusters because the Coulomb energy (4) strongly depends on the fragments positions (see Ref. [40] for details). This is not the case in the present application to neutral clusters because the Coulomb interaction is zero.

3. The weight w_q

The weight w_q takes into account the vibrational excitations and is given by

$$w_q = \prod_{j=1}^{N_f} \int \rho_{vj}(E_{vj}^*) dE_{vj}^*. \qquad (17)$$

In this work, we have assumed that the internal excitation of the clusters is well described within a classical harmonic model. By using this approximation we do not take into account vibrational anharmonicities which can be important for high excitation energies. The sampling of the excitation energies requires the knowledge of the vibrational level density of each fragment $\rho_{vj}(E_{vj}^*)$, which is given by the density of states of a f_{vj}-dimensional harmonic oscillator

$$\rho_{vj}(E_{vj}^*) = \frac{(E_{vj}^*)^{f_{vj}-1}}{\Gamma(f_{vj})\prod_{i=1}^{f_{vj}}(h\nu_{ij})}, \qquad (18)$$

where Γ is Euler's gamma function, f_{vj} is the number of vibrational degrees of freedom of fragment j, and ν_{ij} is the frequency of its ith vibrational mode.

4. The weight w_{pl}

The weight w_{pl} is given by

$$w_{pl} = \int \prod_{j=1}^{N_f} d^{f_{rj}}\mathbf{l}_j \prod_{j=1}^{N_f} d^3\mathbf{p}_j \delta(\mathbf{L} - \mathbf{L}_0)\delta(\mathbf{P} - \mathbf{P}_0)\delta(E - E_0).$$
$$(19)$$

For the sake of simplicity, we will assume that, initially, the cluster does not rotate ($\mathbf{L}_0 = 0$) and is at rest ($\mathbf{P}_0 = 0$). Nevertheless, a major difficulty remains: the second term in Eq. (7) shows that the fragments' positions and linear momenta are correlated (in other words, it is not possible to choose independently these variables). To keep the advantage of a fast numerical scheme, we have made the additional assumption that the second term in Eq. (7) is zero. Then the computation of w_{pl} reduces to the evaluation of the following expression:

$$w_{pl} = \int d^3\mathbf{p}_1 d^3\mathbf{p}_2 \dots d^3\mathbf{p}_{N_f} d^{f_{r1}}\mathbf{l}_1 d^{f_{r2}}\mathbf{l}_2 \dots d^{f_{rN_f}}\mathbf{l}_{N_f}$$
$$\times \delta\left(\sum_j \mathbf{l}_j\right)\delta\left(\sum_j \mathbf{p}_j\right)\delta(E - E_0). \qquad (20)$$

Let E_0' be the total kinetic energy available (translational plus rotational)

$$E_0' = E_0 - (E_C + E_B + E_v^*) = K_t + K_r. \qquad (21)$$

It can be shown that the weight w_{pl} can be written as [25]

$$w_{pl} = \prod_{j=1}^{N_f-1} \prod_{\mu=1}^{f_{rj}+3} \left\{ \left(\frac{2}{\lambda_{\mu j}}\right)^{1/2} \right\} \frac{E_0'^{(\alpha-1)}\pi^\alpha}{\Gamma(\alpha)}, \qquad (22)$$

with

$$\alpha = \frac{1}{2}\left(3N_f - 3 + \sum_{j=1}^{N_f-1} f_{rj}\right) \qquad (23)$$

and

$$\lambda_{\mu j} = m_j^{-1} + \left(m_{N_f} + \sum_{l=1}^{j-1} m_l\right)^{-1}, \quad \mu = 1, 2, 3$$

$$= I_{\mu-3,j}^{-1} + \left(I_{\mu-3,N_f} + \sum_{l=1}^{j-1} I_{\mu-3,l}\right)^{-1},$$

$$\mu = 4, \dots, f_{rj} + 3. \qquad (24)$$

It is worth noticing that for cyclic fragments, Eq. (22) is equivalent to Eq. (51) of Ref. [25].

C. Microcanonical Metropolis sampling

In standard statistical mechanics, microcanonical equilibrium means that every accessible phase-space cell ξ_j at a fixed energy E_0 and other conserved quantities (e.g., linear momentum, angular momentum, etc.) is equally populated. The main idea of the method is that one does not sample all the states uniformly (as in ordinary Monte Carlo calculations), but one moves in small steps towards the most important region of the phase space, i.e., the part having the highest values for the weight w.

The Metropolis algorithm allows one to move in phase space Ω' according to the following procedure [41]. First a

configuration ξ_n is randomly chosen in Ω'. By changing only a few degrees of freedom, a trial state ξ_t is generated and the relative weight $\Pi = w_{\xi_t}/w_{\xi_n}$ is computed. Then a random number $p \in [0,1]$ is sampled from a uniform distribution and the state ξ_n is accepted if $p \leq \Pi$. In this case $\xi_{n+1} = \xi_t$. Otherwise, if $p > \Pi$, the old state ξ_n is recorded as a new state (i.e., $\xi_{n+1} = \xi_n$) and a new trial state is computed again. This procedure is repeated many times and the resulting path for the accepted configurations is called a Markov chain. This procedure has been successfully used to study nuclear fragmentation problems [37] as well as fragmentation of hot atomic metal clusters [25].

Displacements along the Markov chain are done according to the following step sequence.

Step 1. The excitation energy of each fragment is sampled according to a uniform distribution from 0 up to the lowest dissociation energy D_j of the corresponding cluster (see Table I). Then the weight w_q is changed. Furthermore, since E_0' depends on the total excitation energy [see Eq. (21)], the weight w_{pl} is also changed.

Step 2. The position $\mathbf{r}_j$ of each fragment is changed one by one. Thus, w_r is modified as well as E_0' and w_{pl} through E_C in Eq. (21). For neutral or singly charged initial clusters this step is skipped.

Step 3. The composition (N_j, Z_j) of two successive fragments is changed. The two fragments are combined, adding the mass and the charge, and are split again in a new way. Then, the geometry, G_j, the electronic spin, S_{ej}, and the orbital degeneracy, O_{ej}, of the two fragments are sampled randomly among the allowed values included in the mass table. Finally the positions and the excitation energies of the new fragments are modified. In this step, the weights w_{pl}, w_r, w_ϕ, w_e, and w_q are modified. If there is only one fragment, the geometry, the electronic spin and the electronic orbital momentum of the cluster are randomly chosen. w_{pl}, w_ϕ, and w_e are modified.

Step 4. The number of fragments N_f is changed by ± 1. This is done by either splitting one fragment into two or by combining two fragments into one. Again the positions, the excitation energies, the geometries, the electronic spins and orbital momenta of these fragments are renewed. The weights w_{pl}, w_r, w_ϕ, w_q, w_e, and w_{NZ} are changed.

In steps 1 to 4 some of the weights are changed. As mentioned above, acceptance or rejection of the new state is decided according to the value of $\Pi = w_{new}/w_{old}$. In each step, energy conservation (imposed by the microcanonical ensemble) is checked.

Once the region of maximum weight has been reached, the statistical expectation value of the observable F is obtained:

$$\langle F \rangle = \sum_{j=1}^{N} F_j/N, \tag{25}$$

where F_j denotes the values of F at the phase-space points ξ_j along the Markov chain and N is the number of cycles (i.e., the number of times the above four steps are completed). In this average, the initial cycles in the Markov chain must be discarded because they do not lie in the region of maximum weight. Since the number of such cycles is not known *a priori*, one must check invariance of this average for several choices of the initial number of cycles.

D. Caloric curve

The shape of the caloric curve (temperature versus the total energy of the system) provides the best signature of a phase transition of first or second order [42–45] in a finite system. Although temperature does not have a well-defined role in a microcanonical ensemble, we will follow common usage and compute an effective temperature using the standard definition in terms of the microcanonical entropy S and the total energy E_0, namely

$$\frac{1}{T} = \frac{\partial S}{\partial E_0} = \frac{\partial \ln \mathcal{Z}}{\partial E_0} = \left\langle \frac{\alpha - 1}{E_0'} \right\rangle, \tag{26}$$

where $\mathcal{Z}$ is defined after Eq. (1), α is given in Eq. (23), and E_0' is the total translational plus rotational kinetic energy (see Sec. II B 4). When all fragments are either linear or cyclic, the above equation takes the form

$$\frac{1}{T} = \left\langle \frac{f_{tr} - 2}{2E_0'} \right\rangle, \tag{27}$$

where f_{tr} is the total number of translational-rotational degrees of freedom given by $f_{tr} = 3N_f + \sum_{j=1}^{N_f} f_{rj} - 5$ and $f_{tr} = 3N_f + \sum_{j=1}^{N_f} f_{rj} - 6$, respectively.

In general, this definition of the effective temperature as a derivative of the microcanonical entropy is not equivalent to the definition in terms of the mean kinetic energy per cluster degree of freedom [46]. However, due to our neglect of crossed terms in the definition of the system total energy (4) and the statistical weight (11), we do not expect the present results to differ significantly from those obtained from the kinetic energy definition of temperature.

III. THE TIME-DEPENDENT WEISSKOPF EVAPORATION MODEL

As mentioned above, the MMMC method considers the system in internal thermodynamic equilibrium (ergodic assumption) and, therefore, it can only provide information for $t = \infty$. In most experimental works [47], however, branching ratios are determined a few nanoseconds after cluster excitation. This is the typical time of flight for the fragments to reach the detector. For metal clusters excited in slow collisions with atomic targets, the ergodic assumption is not fulfilled [26,48]. This is because the resulting fragments reach the detector before they can use all the available energy. Carbon clusters are usually excited by fast projectiles or energetic laser pulses, which means that there is more energy available compared to the cluster dissociation energy. Therefore, one can expect a more rapid decay of the parent cluster and, therefore, a better fulfillment of the ergodic assumption at the ns scale. To check this assumption under realistic experimental conditions, we have adapted the rate equation model previously introduced by Hervieux *et al.* [26] in which dissociation rate constants are obtained within the sta-

tistical method of Weisskopf. Integration of the corresponding set of time dependent equations will show us the range of validity of the MMMC method in this case.

The model assumes that the initial excitation energy leads to a sequential evaporation of different fragments. Evaluation of the rate constants for monomer and dimer evaporation using the Weisskopf theory has been described in detail in [26]. As the results of the next section will show, trimer evaporation is also extremely important in fragmentation of C_7 and C_9. This possibility has not been considered in previous applications of the Weisskopf formalism.

A. Rate constants

The rate constant for monomer evaporation is given by

$$k_{N,1}(E_N^*) = \frac{\mu_1}{\hbar^3 \pi^2} \int_0^{E_N^* - D_{N,1}} \frac{\rho_{e,1} \rho_{e,N-1}}{\rho_{e,N}}$$

$$\times \frac{\rho_{\nu,N-1}(E_N^* - D_{N,1} - e)}{\rho_{\nu,N}(E_N^*)} \sigma(e) e \, de, \quad (28)$$

where μ_1 is the mass of the evaporated atom, E_N^* is the excitation energy of a cluster of size N, $D_{N,1}$ is the energy required to evaporate a monomer, σ is the cluster geometrical cross section that, in the classical Weisskopf model, is given by $\sigma = \pi R^2$ where R is the cluster radius (see Table I), $\rho_{e,i}$ is the electronic density of states $\rho_{e,i} = (2S_{ei} + 1) O_{ei}$, and $\rho_{\nu,i}$ is the vibrational density of states. The latter has been evaluated in the harmonic approximation using Eq. (18). The average kinetic energy of the evaporated monomer is

$$\bar{e}_{N,1} = \frac{1}{k_{N,1}} \frac{\mu_1}{\hbar^3 \pi^2} \int_0^{E_N^* - D_{N,1}} \frac{\rho_{e,1} \rho_{e,N-1}}{\rho_{e,N}}$$

$$\times \frac{\rho_{\nu,N-1}(E_N^* - D_{N,1} - e)}{\rho_{\nu,N}(E_N^*)} \sigma(e) e^2 de \quad (29)$$

and the average excitation energy for the daughter cluster

$$\bar{E}_{N-1}^* = E_N^* - \bar{e}_{N,1}. \quad (30)$$

The rate constant for dimer evaporation is given by

$$k_{N,2}(E_N^*) = \frac{\mu_2}{\hbar^3 \pi^2} \frac{1}{\hbar \omega_d} \int_0^\alpha dx \int_0^{E_N^* - D_{N,2} - x} \frac{\rho_{e,2} \rho_{e,N-2}}{\rho_{e,N}}$$

$$\times \frac{\rho_{\nu,N-2}(E_N^* - D_{N,2} - e - x)}{\rho_{\nu,N}(E_N^*)} \sigma(e) e \, de, \quad (31)$$

where μ_2 is the reduced mass of the evaporated dimer, $D_{N,2}$ is the energy required to evaporate a dimer, and

$$\alpha = \begin{cases} E_N^* - D_{N,2} & \text{if } E_N^* - D_{N,2} \leq D_{2,1}, \\ D_{2,1} & \text{if } E_N^* - D_{N,2} > D_{2,1}, \end{cases}$$

where $D_{2,1}$ is the dimer dissociation energy. The average kinetic energy and the average vibrational energy of the evaporated dimer are given by

$$\bar{e}_{N,2} = \frac{1}{k_{N,2}} \frac{\mu_2}{\hbar^3 \pi^2} \frac{1}{\hbar \omega_d} \int_0^\alpha dx \int_0^{E_N^* - D_{N,2} - x} \frac{\rho_{e,2} \rho_{e,N-2}}{\rho_{e,N}}$$

$$\times \frac{\rho_{\nu,N-2}(E_N^* - D_{N,2} - e - x)}{\rho_{\nu,N}(E_N^*)} \sigma(e) e^2 de \quad (32)$$

and

$$\bar{x}_{N,2} = \frac{1}{k_{N,2}} \frac{\mu_2}{\hbar^3 \pi^2} \frac{1}{\hbar \omega_d} \int_0^\alpha x dx \int_0^{E_N^* - D_{N,2} - x} \frac{\rho_{e,2} \rho_{e,N-2}}{\rho_{e,N}}$$

$$\times \frac{\rho_{\nu,N-2}(E_N^* - D_{N,2} - e - x)}{\rho_{\nu,N}(E_N^*)} \sigma(e) e \, de, \quad (33)$$

where ω_d is the classical harmonic frequency of the dimer. The average excitation energy of the daughter cluster is defined as

$$\bar{E}_{N-2}^* = E_N^* - \bar{e}_{N,2} - \bar{x}_{N,2}. \quad (34)$$

Finally, the rate constant for trimer evaporation is given by

$$k_{N,3} = \frac{\mu_3}{\pi^2 \hbar^3} \int_0^\beta dx \int_0^{E_N^* - D_{N,3} - x} \frac{\rho_{e,3} \rho_{e,N-3}}{\rho_{e,N}}$$

$$\times \frac{\rho_{\nu,3}(x) \rho_{\nu,N-3}(E_N^* - D_{N,3} - e - x)}{\rho_{\nu,N}(E_N^*)} \sigma(e) e \, de, \quad (35)$$

where μ_3 is the reduced mass of the evaporated trimer, $D_{N,3}$ is the energy required to evaporate a trimer, and

$$\beta = \begin{cases} E_N^* - D_{N,3} & \text{if } E_N^* - D_{N,3} \leq D_{3,1}, \\ D_{3,1} & \text{if } E_N^* - D_{N,3} > D_{3,1}. \end{cases}$$

The average kinetic and vibrational energies of the evaporated trimer are

$$\bar{e}_{N,3} = \frac{1}{k_{N,3}} \frac{\mu_3}{\pi^2 \hbar^3} \int_0^\beta dx \int_0^{E_N^* - D_{N,3} - x} \frac{\rho_{e,3} \rho_{e,N-3}}{\rho_{e,N}}$$

$$\times \frac{\rho_{\nu,3} \rho_{\nu,N-3}(E_N^* - E_{N,3} - e - x)}{\rho_{\nu,N}(E_N^*)} \sigma(e) e^2 de \quad (36)$$

and

$$\bar{x}_{N,3} = \frac{1}{k_{N,3}} \frac{\mu_3}{\pi^2 \hbar^3} \int_0^\beta x dx \int_0^{E_N^* - D_{N,3} - x} \frac{\rho_{e,3} \rho_{e,N-3}}{\rho_{e,N}}$$

$$\times \frac{\rho_{\nu,3} \rho_{\nu,N-3}(E_N^* - E_{N,3} - e - x)}{\rho_{\nu,N}(E_N^*)} \sigma(e) e \, de, \quad (37)$$

respectively. The average excitation energy of the daughter cluster is

$$\bar{E}_{N-3}^* = E_N^* - \bar{e}_{N,3} - \bar{x}_{N,3}. \quad (38)$$

In all the above formulas, rotation of the different fragments is not taken into account.

B. Sequential model of evaporation

We illustrate our procedure for the case of C_5 fragmentation. In this case, sequential evaporation follows this scheme:

$$\begin{array}{c}
\text{C}_3 + \text{C} + \text{C} \xrightarrow{k_{3,1}^{(5-1-1)}} \text{C}_2 + 3\text{C} \\[6pt]
\nearrow {\scriptstyle k_{4,1}^{(5-1)}} \\[2pt]
\text{C}_4 + \text{C} \\
\nearrow {\scriptstyle k_{5,1}^{(5)}} \qquad \searrow {\scriptstyle k_{4,2}^{(5-1)}} \\[2pt]
\text{C}_5 \qquad\qquad \text{C}_2 + \text{C}_2 + \text{C} \longrightarrow \cdots \\
\searrow {\scriptstyle k_{5,2}^{(5)}} \\[4pt]
\text{C}_3 + \text{C}_2 \xrightarrow{k_{3,1}^{(5-2)}} \text{C}_2 + \text{C} + \text{C}_2 \longrightarrow \cdots
\end{array}$$

$$(39)$$
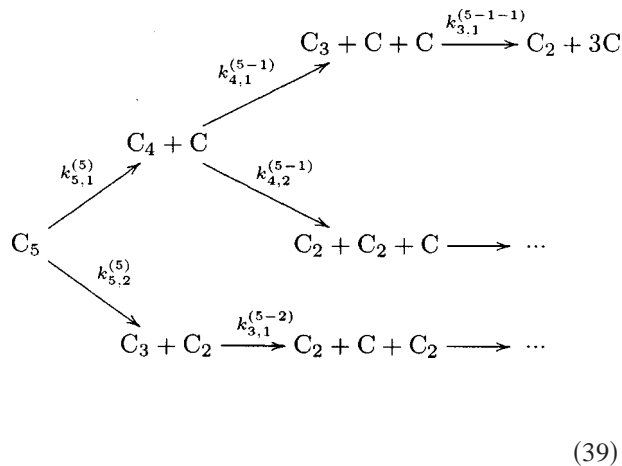
where the rate constant $k_{N,i}^{(k)}$ along the path (k) is evaluated as explained above (for simplicity, fragmentation steps leading to the complete atomization of cluster have been omitted from the diagram). The corresponding system of rate equations is

$$\frac{dn_5^{(5)}}{dt} = -n_5^{(5)}(k_{5,1}^{(5)} + k_{5,2}^{(5)}), \qquad (40)$$

$$\frac{dn_4^{(5-1)}}{dt} = n_5^{(5)}k_{5,1}^{(5)} - n_4^{(5-1)}(k_{4,1}^{(5-1)} + k_{4,2}^{(5-1)}), \qquad (41)$$

$$\frac{dn_3^{(5-2)}}{dt} = n_5^{(5)}k_{5,2}^{(5)} - n_3^{(5-2)}k_{3,1}^{(5-2)}, \qquad (42)$$

$$\frac{dn_3^{(5-1-1)}}{dt} = n_4^{(5-1)}k_{4,1}^{(5-1)} - n_3^{(5-1-1)}k_{3,1}^{(5-1-1)}, \qquad (43)$$

$$\frac{dn_2^{(5-1-2)}}{dt} = n_4^{(5-1)}k_{4,2}^{(5-1)}, \qquad (44)$$

$$\frac{dn_2^{(5-2-1)}}{dt} = n_3^{(5-2)}k_{3,1}^{(5-2)}, \qquad (45)$$

$$\frac{dn_2^{(5-1-1-1)}}{dt} = n_3^{(5-1-1)}k_{3,1}^{(5-1-1)}, \qquad (46)$$

where $n_i^{(k)}$ is the number of fragments of size i along the path (k) [see Eq. (39)]. Integration of these equations up to $t = t_{TOF}$, where t_{TOF} is the experimental time of flight, is done analytically.

In the case of C_7, the number of fragmentation paths and, therefore, of rate equations, is much larger. However, the procedure is totally equivalent to that for C_5 and will be omitted for the sake of conciseness. In view of the results presented in the following sections, we have found it unnecessary to apply this formalism to C_9.

IV. *AB INITIO* STRUCTURE CALCULATIONS

The basic ingredients of the statistical models used in this paper are the geometries, the harmonic frequencies, and the binding energies of all the fragments. In the Metropolis Monte Carlo simulations, the rotational constants are also needed. To obtain this information for all possible fragments, we have applied the density functional theory (DFT) using a hybrid B3LYP functional for exchange and correlation. This DFT approach combines the Becke's three parameter nonlocal hybrid exchange potential [49] with the nonlocal correlation functional of Lee, Yang, and Parr [50]. The geometries of the C_n clusters ($n \leqslant 9$) have been optimized by using the $6-311+\text{G}(3df)$ basis set. We have considered linear and cyclic isomers and singlet and triplet spin multiplicities. The harmonic vibrational frequencies of the different species have been calculated at the same level of theory. The B3LYP functional has been proved to be a good choice for the description of carbon clusters [51]. In the case of small carbon clusters, the calculated geometries and the vibrational frequencies are very close to those obtained at higher levels of calculation [28,29,52].

The electronic and binding energies have been obtained with the coupled cluster theory $\text{CCSD(T)}/6-311+\text{G}(3df)$, which includes all single and double excitations, as well as triple excitations in a perturbative way [53], and made use of the B3LYP optimized geometry. The electronic energies obtained at this level of theory have been corrected with the zero point energy (ZPE) values obtained from the DFT vibrational analysis. All calculations have been performed with the Gaussian-98 program [54].

In Table I we show the results of the electronic structure calculations for neutral carbon clusters from C_1 up to C_9 considering linear and cyclic geometries and singlet and triplet spin multiplicities for each conformer. In this table the electronic energy at the $\text{CCSD(T)}/6-311+\text{G}(3df)$ level of theory including the ZPE correction is shown as well as other variables introduced in the dynamical calculations. In particular, the table includes the geometrical average of the harmonic frequencies and the principal moments of inertia I_1, I_2, and I_3 of the fragment. The cluster radius R has been defined as half the largest distance between two C atoms in a given fragment. The table also includes the dissociation energy D corresponding to the lowest fission channel. The last column in this table is $\ln(\rho)$, where $\rho_j = D^{f_{vj}-1}/(\Gamma(f_{vj})\bar{\nu}_j^{f_{vj}})$; this value is an indication of the weight w_q. This table, known as the mass table, includes all the required data for the statistical calculations.

In agreement with previous theoretical calculations [29], the most stable C_n isomer ($n = 3$, 5, 7, and 9) corresponds to the linear isomer with singlet spin multiplicity. However, the ground state of the C_4, C_6, and C_8 clusters is still an open question. In agreement with previous results [27,31], our coupled cluster calculations for C_4 predict the cyclic structure as the most stable one, but multireference configuration interaction calculations (MRCI) [33] shows that the ground state of C_4 corresponds to a triplet linear structure with an energy 4.1 kcal/mol below the cyclic one. Previous theoretical results for C_6 and C_8 [30,32,34,35] lead to identical conclusions: multireference calculations predict the cyclic structure to be the most stable one while the coupled cluster theory predicts the opposite. In practice, both isomeric forms (linear and cyclic) are nearly degenerate. In our MMMC
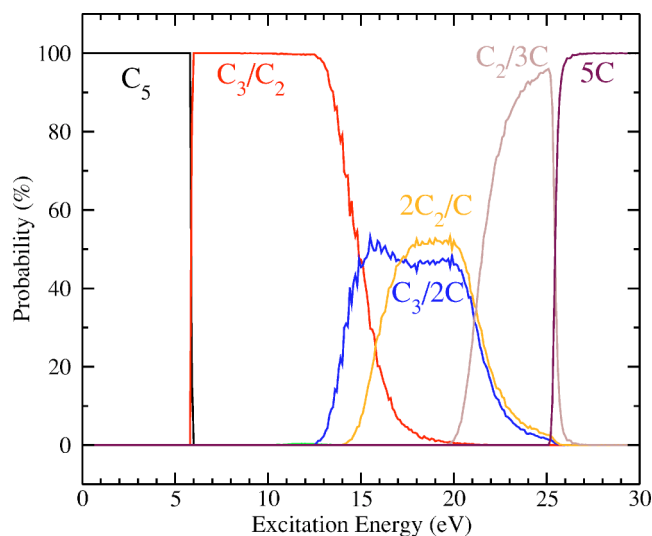
FIG. 1. (Color online) Fragmentation of C_5 from MMMC simulations. Channel probabilities as functions of excitation energy.

simulations, we have introduced *all* isomeric forms (linear and cyclic geometries and singlet and triplet multiplicities) for C_n ($n=2-9$). Therefore, all species that can play an important role in fragmentation are taken into account.

V. RESULTS AND DISCUSSION

We first present our results for the fragmentation branching ratios of C_5. The excited C_5 cluster may follow seven fragmentation channels [see Eq. (39)]: C_4/C, C_3/C_2, $C_3/C/C$; $C_2/C_2/C$; $C_2/C/C/C$; $C/C/C/C/C$. Figure 1 shows the corresponding fragmentation probabilities as functions of cluster excitation energy obtained from MMMC simulations. These results are close to those reported in [5]. The C_5 cluster does not dissociate up to 6 eV. In the range of excitation energy ∼6–15 eV, the C_3/C_2 channel is dominant in agreement with previous photodissociation [20] and collision induced dissociation [21] experiments. As already mentioned, C_3 loss is also the most probable process in fragmentation of positively and negatively charged carbon clusters [6–19]. The other competing channel leading to two fragments (C_4/C) has a negligible probability in the whole energy range. Since the C_3/C_2 channel requires less energy than the C_4/C one, we can conclude that it is the high stability of C_3 that governs the observed decay in this energy region. From 15 to 22 eV, only the two channels leading to three fragments play a significant role: $C_3/2C$ and $2C_2/C$. The four fragment channel $C_2/3C$ appears at 20 eV and is the dominant one at 23 eV. The C_5 cluster is completely broken in 5C (five fragment channel) at 25 eV. When the number of fragments change from one to two and from four to five the variation in the branching ratios is drastic. This variation is smoother in the energy region from 10–25 eV. This fact shows that not only energy considerations, but also entropy factors are important to describe fragmentation. This is also one of the reasons why the probability to observe the C_4/C channel is practically zero even at high excitation energies where more than two fragments are produced.
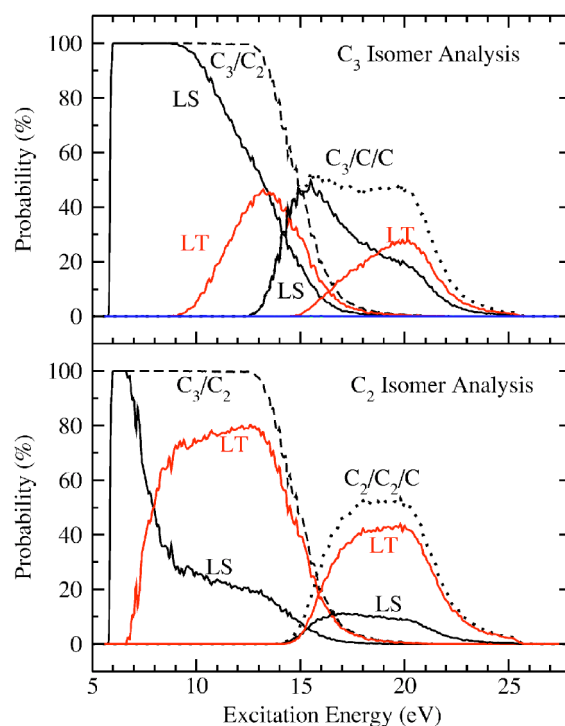
FIG. 2. (Color online) Isomer analysis of the C_3/C_2, $C_3/C/C$, and $C_2/C_2/C$ channels in C_5 fragmentation. Discontinuous lines represent channel probabilities. LS, linear singlet; LT, linear triplet; CS, cyclic singlet; CT, cyclic triplet.

We have analyzed the isomer composition in the dominant fragmentation channels. This is shown in Fig. 2. Although we have run our simulations taking the linear singlet C_5 isomer as the starting point, the isomer analysis just below the lowest dissociation threshold reveals a mixture of four species: ∼25% linear singlet, ∼25% linear triplet, ∼25% cyclic singlet, and ∼25% cyclic triplet (not shown in the figure). We have checked that starting the simulations with a different C_5 isomer barely changes these percentages. The isomer analysis corresponding to the C_3/C_2 channel is shown in Fig. 2. Dashed and dotted lines reproduce the C_3/C_2 and $C_3/C/C$ channel probabilities shown in Fig. 1. Our results point out that only the linear C_3 isomers play a significant role in both channels. Cyclic isomeric forms of C_3 are never observed. Isomers with singlet multiplicities are more important in the low energy regions of the C_3/C_2 and $C_3/C/C$ channels, while isomers with triplet multiplicities are relevant at higher energies. In particular, the two maxima observed in the $C_3/C/C$ probability are due to the smooth transition from a dominant singlet linear structure to a dominant triplet linear structure. The analysis of the different C_2 isomers shown in the bottom of the figure reveals that the triplet multiplicity is dominant except between 5 and 7 eV. Although not shown in the figure, a similar analysis shows that atomic carbon always appears with dominant triplet multiplicity.

As explained above, the MMMC results are obtained under the assumption of internal thermodynamic equilibrium. However, we would like to compare our results with experimental branching ratios obtained in collision experiments
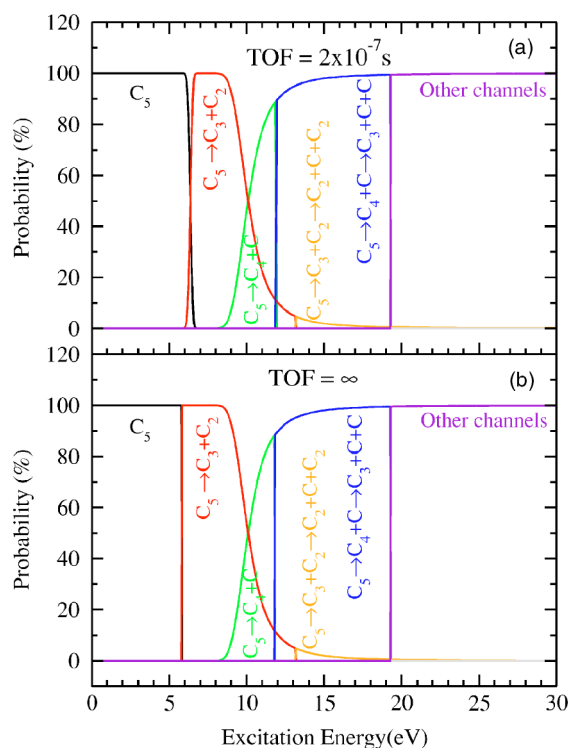
FIG. 3. (Color online) Time dependent Weisskopf calculations of C_5 fragmentation for (a) TOF=2×10^{-7} s and (b) TOF=∞.

with a time of flight (TOF) of $\sim$180 ns [21]. In order to be confident that the experimental conditions are compatible with the assumption of internal thermodynamic equilibrium, we have performed time dependent Weisskopf simulations as described in Sec. III. To simplify the latter calculations we have only considered the dominant isomeric species. According to the analysis presented in Fig. 2, these are linear structures with either singlet or triplet spin multiplicity. We have performed our calculations for two values of the TOF: the experimental value (180 ns) and TOF=∞. The results are shown in Figs. 3(a) and 3(b). The most significant difference between both figures is a small shift (less than 1 eV) in the appearance of the $C_5 \rightarrow C_3 + C_2$ path. Therefore, we can conclude that the experimental conditions of [5,21] are compatible with the use of MMMC method to analyze the observed fragmentation. However, if we compare the probabilities calculated with the Weisskopf method at TOF=∞ with those obtained with the MMMC method (Fig. 1), we can see significant discrepancies. For instance, the C_4/C channel does not appear in the MMMC calculations, while it has a substantial probability in the Weisskopf calculations between 10 and 12 eV. Although the treatment of the vibrational density of states in both methods is identical, rotational effects have been excluded in our implementation of the Weisskopf method. To check if this is the origin of the discrepancy, we have carried out MMMC simulations in which all rotational factors have been excluded from the corresponding statistical weights. The results of these MMMC simulations are shown in Fig. 4. These results agree reasonably well with those obtained with the Weisskopf method at TOF=∞ (see Fig. 3). This proves that rotational effects play a very important role
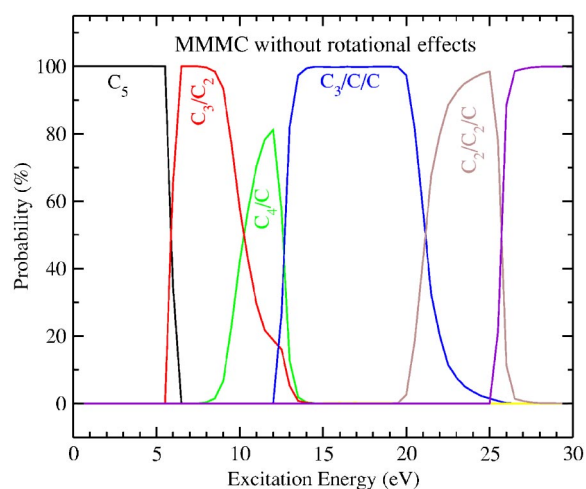
FIG. 4. (Color online) MMMC simulation for C_5 fragmentation without rotational effects.

in the fragmentation process and that our previous conclusion, namely that the experimental conditions are compatible with the use of MMMC method, is still valid.

In the case of C_7, the number of fragmentation channels is fifteen. The results of the MMMC simulations are shown in Fig. 5; they are close to those reported in [5]. Fragmentation is observed above 6 eV. As for C_5, the dominant dissociation channel at low energies is C_{n-3}/C_3. Nevertheless, in the energy range 6–13 eV, the C_5/C_2 channel is also observed and competes efficiently with the C_4/C_3 channel. The probability of the C_6/C channel is practically zero. The high stability of C_3 explains the large probabilities of all fragmentation channels that contain this cluster. For example, in the energy region where three fragment channels appear ($\sim$14–25 eV), only those containing C_3 are visible: C_3/C_3/C and C_3/C_2/C_2. These two channels are in strong competition around 20 eV. There is almost no trace of the C_5/C/C and C_4/C_2/C channels. Above 25 eV dissociation channels with
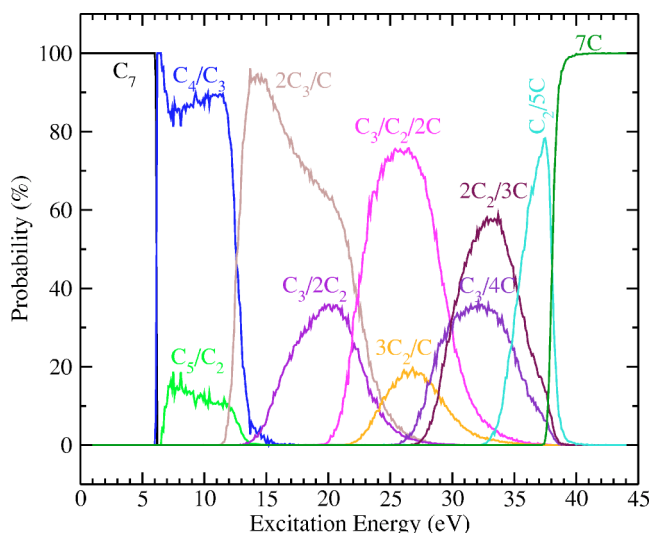
FIG. 5. (Color online) Fragmentation of C_7 from MMMC simulations. Channel probabilities as functions of excitation energy.
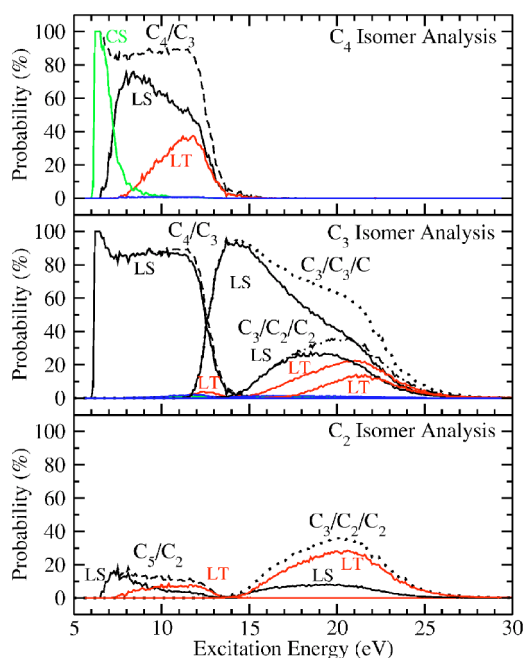
FIG. 6. (Color online) Isomer analysis of the dominant dissociation channels in C_7 fragmentation. Discontinuous lines represent channel probabilities. Labels as defined in Fig. 2.

FIG. 7. (Color online) Weisskopf calculations for C_7 fragmentation using (a) TOF=2×10^{-7} s and (b) TOF=∞.

four, five, and six fragments present maximum probabilities between 20 and 70%. The C_7 cluster is completely broken into seven carbon atoms at ~40 eV. Although fragmentation of C_7 is more complicated than that of C_5, we see again that decay channels leading to C_3 are favored. The absence of the C_6/C, $C_5/C/C$, $C_4/C_2/C$,…, channels at high energies is again due to entropic factors.

In this case, we have also analyzed the isomer composition of the dominant fragmentation channels. The results are shown in Fig. 6. Discontinuous lines represent the channel probabilities given in Fig. 5. The composition of the parent cluster before fragmentation (not shown in the figure) is ~25% for each possible structure (linear or cyclic geometry with singlet or triplet spin multiplicity). For the C_4/C_3 channel we see that the peak at ~7 eV is due to the dominance of the C_4 cyclic form with singlet spin multiplicity. C_3 linear isomers successively appear as the energy increases, being the singlet isomer the most important one. This result shows the importance of including all possible isomers in the simulation, especially when they are energetically degenerate as for the linear and cyclic structures of C_4. The C_3 isomer analysis in the same channel shows that the cyclic structures do not play any role in the fragmentation and that the linear isomer with singlet multiplicity is the dominant structure. The composition study of the C_5/C_2 channel (not shown in the figure) indicates that the C_5 cluster has always linear geometry and singlet multiplicity, however Fig. 6 shows that singlet and the triplet species compete for C_2. The $C_3/C_3/C$ probability exhibits a shoulder at 22 eV. This can be well understood by examination of the C_3 isomer composition: Figure 6 shows that the probabilities associated with the singlet and triplet linear structures of C_3 meet at this energy. Atomic carbon produced in this channel correspond to the
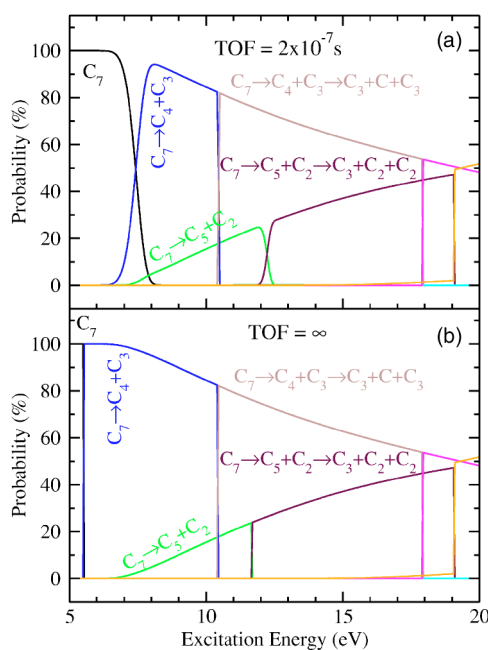
triplet multiplicity. In the case of the $C_3/C_2/C_2$ channel, the asymmetric shape of the corresponding probability is again due to the competition between the singlet and triplet linear structures of C_3 (they meet at ~22 eV). The singlet isomer appears at lower excitation energies while the triplet one becomes dominant at higher energies. The C_2 analysis shows that the triplet isomer is the dominant one in this channel.

We have also carried out time dependent fragmentation calculations for C_7 based on the Weisskopf theory. In these calculations we have only considered the most stable isomer for each fragment. The results are shown in Fig. 7. We can see that the results for the experimental value of the TOF (~200 ns) and TOF=∞ are very similar. The only difference is a shift of ~2 eV in the C_4/C_3 threshold. So, as for C_5, the use of the MMMC method is compatible with the experimental conditions.

We move now to the C_9 cluster. In this case, there are thirty fragmentation channels. The results obtained with the MMMC simulations are shown in Fig. 8. These results differ somewhat from those reported in [5] for a large number of fragments but are very close to them for excitation energies below 20 eV. As in previous cases, the most favorable dissociation channels involve C_3 formation, for example, C_6/C_3 and $C_3/C_3/C_3$. In this case, many fragmentation channels compete efficiently in the energy range up to the total atomization of the cluster at ~53 eV. We have also checked that inclusion of rotational effects is essential in this case since, by removing these effects from the corresponding weights, we obtain quite different results. For example, C_8/C would appear as a dominant channel while it is not observed in experiments (see below).

The isomer analysis for the dominant fragmentation channels is shown in Fig. 9. In the C_6/C_3 channel, the dominant species are the triplet linear structure of C_6 and the singlet linear structure of C_3. The latter is also the dominant struc-

FIG. 8. (Color online) Fragmentation of C_9 from MMMC simulations. Channel probabilities as functions of excitation energy.

ture in the $C_3/C_3/C_3$ and the $2C_3/C_2/C$ channels, although the triplet linear structure has some relevance in the high energy parts of these channels. As in the cases discussed above, the C_9 channel is almost a statistical mixture of the four isomers included in our simulations. Also, the dominant form of C_2 is the linear triplet one.

A common feature in the three systems is the dominance of the linear fragments (LT and LS) with respect to the cyclic ones. This is because the weight w_q, which measures the accessible vibrational states, is always larger for the linear species than for the cyclic ones. This is illustrated in the last column of Table I, which gives the logarithm of the density

FIG. 9. (Color online) Isomer analysis of the dominant dissociation channels in C_9 fragmentation. Discontinuous lines represent channel probabilities. Labels as defined in Fig. 2.

FIG. 10. (Color online) Effective temperature as a function of excitation energy (left *y* axis). Discontinuous lines represent channel probabilities (right *y* axis).

of vibrational states at an energy D. Cyclic structures have a lower value of the density of states because, in general, they are more rigid than the linear ones and, therefore, they have a larger average vibrational frequency (see $\bar{\nu}$ column in Table I). The importance of including rotational effects to correctly reproduce the fragmentation branching ratios (see our previous discussion on Fig. 4) is the consequence of the dominant role of the linear structures. Cyclic species are closer to a spherical shape and, consequently, rotation about different directions in space does not introduce significant effects.

Figure 10 shows the variation of the effective temperature as a function of the cluster excitation energy for the three cases investigated here. The behavior of these caloric curves is monotonous except in the regions where new decay channels are open. The observed "plateaus" and oscillations can be interpreted as the signature of first order phase transitions. For C_5, phase transitions are very marked at all intermediate steps of the fragmentation process. In all cases, the phase transitions are more apparent when total atomization of the parent cluster is produced. The latter process occurs around $T=0.4$ eV, which is close to the boiling temperature of macroscopic liquid carbon: $T_b=0.44$ eV. Phase transitions associated with partial fragmentation of the parent cluster are apparent due to the finite size of the system: the larger the cluster, the closer to the infinite size behavior.

The slope of the curves shown in Fig. 10 is usually interpreted as the inverse of the cluster heat capacity. It can be seen that, in short ranges of temperature in the region of phase transitions, the heat capacity can be negative. This effect, which cannot occur in bulk matter, has been recently observed in several experiments on alkali [42,55] and hydro-

FIG. 11. (Color online) Branching ratios for deexcitation of C_5, C_7, and C_9 clusters. Full circles: experiment; open squares: convolution of the theoretical branching ratios with the energy distributions given in Ref. [5]. For C_9, the figure does not include channels leading to five or more fragments because the corresponding ratios are smaller than 1%.

gen [43,44] clusters, and has been explained in terms of two effective temperatures corresponding to solid and liquid aggregate states [46,56]. The present results suggest that negative heat capacities are a general feature of any cluster undergoing a phase transition [57].

VI. COMPARISON WITH EXPERIMENT

Very recently, fragmentation of neutral C_n clusters ($n = 5, 7, 9$) has been investigated experimentally [5]. In these experiments, neutral C_n clusters were produced by charge transfer in fast collisions of C_n^+ ions with a helium gas. The neutral species formed immediately after the collision are electronically excited, which induces fragmentation. The measured branching ratios are shown in Fig. 11. The main problem in these experiments is that the excitation energy resulting from the collision is unknown. This is a very important limitation to understand the observed fragmentation because, as shown in the previous section, the fragmentation branching ratios strongly depend on the excitation energy. Nevertheless, a qualitative inspection of Fig. 11 shows that, in agreement with our theoretical findings, fragmentation channels leading to C_3 are strongly favored. Comparison of these results with our MMMC simulations of Figs. 1, 5, and 8 shows that, for the three systems investigated in this work, theory and experiment are compatible if one assumes that the energy distribution of the neutral cluster just after the collision has a maximum around 10 eV and a width of the order

of 10 eV. A more careful comparison between theory and experiment has been reported in Ref. [5], where the calculated probabilities were convoluted using an empirical function for the energy distribution. The latter function was chosen to give the best fit of the experimental data (see [5] for details). We have repeated this procedure here. The results of such convolutions are shown in Fig. 11. They are practically undistinguishable from those reported in [5]. As can be seen, the general agreement with experiment is good. The most visible discrepancies are obtained for C_9, in particular for the C_6/C_3 channel that is overestimated. As in Ref. [5], an important conclusion of this comparison is that the energy distribution is practically identical for the three systems C_5, C_7, and C_9. This is relevant because the three fits were performed separately. Moreover, this is consistent with the conditions used in the experiments. Indeed the collision velocity and the cluster initial temperature are nearly the same in the three experiments and, therefore, one would expect a similar collisional excitation of the neutral C_n clusters formed in the charge transfer reaction.

VII. CONCLUSIONS

We have applied the microcanonical Metropolis Monte Carlo (MMMC) and the time dependent Weisskopf methods to investigate fragmentation of highly excited small neutral carbon clusters, namely C_5, C_7, and C_9. The necessary microscopic information required to apply both methods has been obtained from state-of-the-art *ab initio* quantum chemistry calculations. In these calculations all possible fragmentation channels, including different isomeric forms (linear and cyclic) and spin multiplicities have been considered. By comparing results of the MMMC and Weisskopf methods, we have checked that, for the present applications, the assumption of internal thermodynamic equilibrium (a necessary condition to apply the MMMC method) is well fulfilled when the time of flight for detection of the different fragments is of order of a few nanoseconds or larger. The analysis of the different isomeric forms included in the MMMC calculations illustrates that competition between different structures of a given fragment is possible and affects the observed branching ratios. We have also demonstrated that inclusion of rotational effects is crucial to obtain a reasonable description of the fragmentation process.

For the three systems investigated here, we have found that channels leading to the formation of C_3 play a dominant role, in particular the C_{n-3}/C_3 channel is always dominant for a range of excitation energies that goes from the corresponding dissociation threshold up to the energy region where fragmentation into three or more species is possible. Among the different isomeric forms of C_3, the linear structure is the most important one. We have compared our calculated branching ratios with the experimental results of Martinet *et al.* [5], who have studied fragmentation of excited neutral C_n clusters produced in the charge transfer reaction $C_n^+ + He \rightarrow C_n + He^+$. The agreement between theory and experiment is reasonably good provided that the theoretical branching ratios are convoluted with a C_n energy distribution centered at around 10 eV. Since the result of the con-

volution is very sensitive to the form of this energy distribution, we conclude that combination of experimental measurements with accurate statistical fragmentation simulations can provide a reasonable estimation of the cluster energy distribution just after the collision.

An interesting prediction of the present study is the existence of phase transitions. These phase transitions could be observed in experiments like those reported in [5] by varying the cluster excitation energy. This can be done, for instance, by using different values of the impact velocity. So far, all experiments have been performed at a fixed or nearly fixed impact velocity of 2.6 a.u., which leads to an energy deposit of around 10 eV. Our simulations have shown that there is a correspondence between impact velocity and excitation energy. As can be seen in Fig. 10, an energy of 10 eV is too low to observe phase transitions (they are only visible at around 20 eV and above). Thus, a broad range of impact velocities should be considered in the experiments in order to observe this phenomenon.

Despite the successful application of the present MMMC model to understand fragmentation of small carbon clusters, several improvements can still be done to gain in accuracy. First, one should introduce vibrational anharmonicities, which might be important at high excitation energies. Second, the model should account for spin conservation, which has been ignored to simplify the evaluation of the statistical average given in Eq. (9). Finally, the approximations performed to evaluate the weight w_{pl} should be checked in more detail by comparing the results of our model with an "exact" phase space theory or molecular dynamics simulations for a small system [58]. Although we do not expect significant changes, introduction of these refinements might account for the remaining discrepancies with experiment. Work along these lines is in progress in our laboratory.

[1] E. E. B. Campbell and F. Rohmund, Rep. Prog. Phys. **63**, 1061 (2000).

[2] C. Lifshitz, Int. J. Mass. Spectrom. **200**, 423 (2000).

[3] E. E. Campbell, *Fullerene Collision Reactions*, 1st ed. (Kluwer Academic, Dordrecht, 2003).

[4] C. Bréchignac, P. Cahuzac, B. Concina, J. Leygnier, L. F. Ruiz, B. Zarour, P.-A. Hervieux, J. Hanssen, M. F. Politis, and F. Martín, Phys. Rev. A **68**, 063202 (2003).

[5] G. Martinet *et al.*, Phys. Rev. Lett. **93**, 063401 (2004).

[6] P. P. Radi, T. L. Bunn, P. Kemper, M. E. Molchan, and M. T. Bowers, J. Chem. Phys. **88**, 2809 (1988).

[7] P. P. Radi, M. E. Rincon, M. T. Hsu, J. Brodbelt-Lustig, P. Kemper, and M. T. Bowers, J. Chem. Phys. **93**, 6187 (1989).

[8] P. P. Radi, M. E. Rincon, M. T. Hsu, J. Brodbelt-Lustig, P. Kemper, and M. T. Bowers, J. Chem. Phys. **92**, 4817 (1990).

[9] M. E. Geusic, T. J. McIlrath, M. F. Jarrold, L. A. Bloomfield, R. R. Freeman, and W. L. Brown, J. Chem. Phys. **84**, 2421 (1986).

[10] M. E. Geusic, T. J. McIlrath, M. F. Jarrold, L. A. Bloomfield, R. R. Freeman, and W. L. Brown, Z. Phys. D: At., Mol. Clusters **3**, 309 (1986).

[11] M. E. Geusic, M. F. Jarrold, T. J. McIlrath, R. R. Freeman, and W. L. Brown, J. Chem. Phys. **86**, 3862 (1987).

[12] R. Bouyer, F. R. Monchicourt, M. Perdix, and P. Pradel, J. Chem. Phys. **100**, 8912 (1994).

[13] K. B. Shelimov, J. M. Hunter, and M. F. Jarrold, Int. J. Mass Spectrom. Ion Processes **138**, 17 (1994).

[14] M. B. Sowa, P. A. Hinz, and S. L. Anderson, J. Chem. Phys. **95**, 4719 (1991).

[15] C. Lifshitz, T. Peres, S. Kababia, and I. Agranat, Int. J. Mass Spectrom. Ion Processes **82**, 193 (1988).

[16] C. Lifshitz, T. Peres, and I. Agranat, Int. J. Mass Spectrom. Ion Processes **93**, 149 (1989).

[17] C. Lifshitz, H. F. G. P. Sandler, J. Sun, T. Weiske, and H. Schwart, J. Phys. Chem. **97**, 6592 (1993).

[18] S. W. McElvany, Int. J. Mass Spectrom. Ion Processes **102**, 81 (1990).

[19] Y. Tai, J. Murakami, Y. Maruyama, W. Yamaguchi, T. Mizota, K. Igarashi, and S. Tanemura, J. Phys. Chem. B **103**, 5500 (1999).

[20] H. Choi, R. T. Bise, A. A. Hoops, D. H. Mordaunt, and D. M. Neumark, J. Phys. Chem. **104**, 2025 (2000).

[21] M. Chabot *et al.*, Nucl. Instrum. Methods Phys. Res. B **197**, 155 (2002).

[22] R. T. Chancey, L. Oddershede, F. E. Harris, and J. R. Sabin, Phys. Rev. A **67**, 043203 (2003).

[23] H. O. Jeschke, M. E. Garcia, and J. A. Alonso, Chem. Phys. Lett. **352**, 154 (2002).

[24] S. Wearasinghe and F. G. Amar, J. Chem. Phys. **98**, 4967 (1993).

[25] D. H. E. Gross and P. A. Hervieux, Z. Phys. D: At., Mol. Clusters **35**, 27 (1995).

[26] P. A. Hervieux, B. Zarour, J. Hanssen, M. F. Politis, and F. Martín, J. Phys. B **34**, 3331 (2001).

[27] J. M. L. Martin, J. P. François, and R. Gijbels, J. Chem. Phys. **94**, 3753 (1991).

[28] J. M. L. Martin, J. El-Yazal, and J. P. François, Chem. Phys. Lett. **242**, 570 (1995).

[29] J. M. L. Martin, J. El-Yazal, and J. P. François, Chem. Phys. Lett. **252**, 9 (1996).

[30] J. M. L. Martin and P. R. Taylor, J. Phys. Chem. **100**, 6047 (1996).

[31] J. D. Watts, J. Gauss, J. F. Stanton, and R. J. Barlett, J. Chem. Phys. **97**, 8372 (1992).

[32] V. Parasuk and J. Almlöf, J. Chem. Phys. **91**, 1137 (1989).

[33] V. Parasuk and J. Almlöf, J. Chem. Phys. **94**, 8172 (1991).

[34] V. Parasuk and J. Almlöf, Theor. Chim. Acta **83**, 227 (1992).

[35] J. Hutter and H. P. Lüthi, J. Chem. Phys. **101**, 2213 (1994).

[36] A. V. Orden and R. J. Saykally, Chem. Rev. (Washington, D.C.) **98**, 2313 (1998).

[37] D. H. E. Gross, Rep. Prog. Phys. **53**, 605 (1990).

[38] G. E. Andrews, *Encyclopedia of Mathematics and its Applications* (Cambridge University Press, Cambridge, England, 1976).

[39] L. D. Landau and E. M. Lifshitz, *Statistical Physics* (Pergamon, Oxford, 1969).

[40] O. Schapiro, P. J. Kuntz, K. Möhring, P. A. Hervieux, M. Madjet, and D. H. E. Gross, Z. Phys. D: At., Mol. Clusters **41**, 219 (1997).

[41] N. Metropolis, A. W. Rosenbluth, M. N. Rosenbluth, A. H. Teller, and E. Teller, J. Chem. Phys. **21**, 1087 (1953).

[42] M. Schmidt, T. Hippler, J. Donges, W. Kronmüller, B. von Issendorff, H. Haberland, and P. Labastie, Phys. Rev. Lett. **87**, 203402 (2001).

[43] F. Gobet, B. Farizon, M. Farizon, M. J. Gaillard, J. P. Buchet, M. Carré, and T. D. Märk, Phys. Rev. Lett. **87**, 203401 (2001).

[44] F. Gobet, B. Farizon, M. Farizon, M. J. Gaillard, J. P. Buchet, M. Carré, P. Scheier, and T. D. Märk, Phys. Rev. Lett. **89**, 183403 (2002).

[45] C. Bréchignac, P. Cahuzac, B. Concina, and J. Leygnier, Phys. Rev. Lett. **89**, 203401 (2002).

[46] R. S. Berry and B. M. Smirnov, JETP **114**, 6816 (2004).

[47] C. Bréchignac, P. Cahuzac, B. Concina, J. Leygnier, L. F. Ruiz, B. Zarour, P.-A. Hervieux, J. Hanssen, M. F. Politis, and F. Martín, Phys. Rev. Lett. **89**, 183402 (2002).

[48] B. Zarour, J. Hanssen, P.-A. Hervieux, M. F. Politis, and F. Martín, J. Phys. B **33**, L707 (2000).

[49] A. D. Becke, J. Chem. Phys. **98**, 5648 (1993).

[50] C. Lee, W. Yang, and R. G. Parr, Phys. Rev. B **37**, 785 (1988).

[51] S. Díaz-Tendero, M. Alcamí, and F. Martín, J. Chem. Phys. **119**, 5545 (2003).

[52] S. Díaz-Tendero, F. Martín, and M. Alcamí, J. Phys. Chem. **106**, 10782 (2002).

[53] *Recent Advances in Coupled-Cluster Theory*, edited by R. J. Bartlett (World Scientific, Singapore, 1997).

[54] M. J. Frisch *et al.*, Gaussian 98, Revision A.11, Gaussian Inc., Pittsburgh, PA, 2001.

[55] M. Schmidt, R. Kusche, B. von Issendorff, and H. Haberland, Nature (London) **393**, 238 (1998).

[56] R. S. Berry and B. M. Smirnov, J. Chem. Phys. **114**, 6816 (2001).

[57] D. H. E. Gross, Phys. World **16**(11), 23 (2004).

[58] F. Calvo and P. Parneix, J. Chem. Phys. **119**, 256 (2003).